

## PAPER

[View Article Online](#)  
[View Journal](#) | [View Issue](#)

# Taming microwave plasma to beat thermodynamics in CO<sub>2</sub> dissociation

G. J. van Rooij,<sup>\*a</sup> D. C. M. van den Bekerom,<sup>a</sup> N. den Harder,<sup>a</sup> T. Minea,<sup>a</sup> G. Berden,<sup>b</sup> W. A. Bongers,<sup>a</sup> R. Engeln,<sup>c</sup> M. F. Graswinckel,<sup>a</sup> E. Zoethout<sup>a</sup> and M. C. M. van de Sanden<sup>ac</sup>

Received 29th April 2015, Accepted 10th June 2015

DOI: 10.1039/c5fd00045a

The strong non-equilibrium conditions provided by the plasma phase offer the opportunity to beat traditional thermal process energy efficiencies *via* preferential excitation of molecular vibrations. Simple molecular physics considerations are presented to explain potential dissociation pathways in plasma and their effect on energy efficiency. A common microwave reactor approach is evaluated experimentally with Rayleigh scattering and Fourier transform infrared spectroscopy to assess gas temperatures (exceeding 10<sup>4</sup> K) and conversion degrees (up to 30%), respectively. The results are interpreted on a basis of estimates of the plasma dynamics obtained with electron energy distribution functions calculated with a Boltzmann solver. It indicates that the intrinsic electron energies are higher than is favorable for preferential vibrational excitation due to dissociative excitation, which causes thermodynamic equilibrium chemistry to dominate. The highest observed energy efficiencies of 45% indicate that non-equilibrium dynamics had been at play. A novel approach involving additives of low ionization potential to tailor the electron energies to the vibrational excitation regime is proposed.

## 1 Introduction

The emission of carbon dioxide into the atmosphere is widely regarded as a severe environmental issue due to concern over its effect on climate change. The consequent increasingly stronger limits on CO<sub>2</sub> exhausts are driving the transition to sustainable energy sources. The intermittent character of, particularly, solar photovoltaics and wind imposes the need for energy storage. At the same time, these sustainable energy sources produce electricity, whereas, globally, less

<sup>a</sup>Dutch Institute for Fundamental Energy Research, P.O. box 6336, 5600 HH Eindhoven, The Netherlands. E-mail: g.j.vanrooij@differ.nl; Tel: +31 40 333 49 99

<sup>b</sup>Radboud University, Institute for Molecules and Materials, FELIX Laboratory, Toernooiveld 7c, 6525 ED Nijmegen, The Netherlands

<sup>c</sup>Department of Applied Physics, Plasma and Materials Processing Group, Eindhoven University of Technology, P.O. Box 513, 5600 MB Eindhoven, The Netherlands

than 20% of the energy is consumed in that form. Converting temporary electrical energy surpluses into chemical fuels would, thus, be advantageous in view of energy density as well as to address CO<sub>2</sub> emissions in other areas of energy consumption (*e.g.* transportation). A promising approach for this conversion involves the non-equilibrium chemistry in the plasma phase. The present paper deals with the particular case of plasma chemical CO<sub>2</sub> reduction as the first step in the production of carbon-based fuels.

Electrical discharges are usually sustained by electric fields through which energy is, in the first instance, transferred to the free electrons. Subsequently, this energy is transferred by collisions to the (neutral) gas phase heavy particles (*e.g.* CO<sub>2</sub> molecules). Due to the large mass difference between collision partners, the elastic energy transfer is inefficient and hence there may be large differences between their temperatures. It is under such far from thermodynamic equilibrium conditions that it is possible to intensify traditional chemical processes and to achieve the highest energy efficiencies.<sup>1</sup>

If the energy of the electrons is high enough, the heavy gas particles may be excited into higher electronic states or even be ionized. Ionization is required for sustaining the plasma discharge. However, in the present context, the subsequent dissociative recombination should not become the dominant pathway to dissociation as it is energetically an inefficient way of initiating chemical reactions. After all, ionization of CO<sub>2</sub> requires  $\sim 14$  eV per molecule, whereas its “net” dissociation energy is  $\sim 3$  eV (considering the “net” reaction  $\text{CO}_2 \rightarrow \text{CO} + \frac{1}{2} \text{O}_2$ ). This consideration implies a 20% maximum energy efficiency for dissociation *via* ionization.

On the other hand, low energy electron collisions can excite vibrational modes in the molecule. Such vibrationally excited molecules will further interact with each other, collisionally exchanging vibrational energy up along the energy scale until the dissociation limit is reached. In this scheme, the electrons, that were energetically “expensive” to create, are used many times to deliver energy specifically to the bonds that are to be broken up to the point where dissociation of the molecule is achieved. It is this qualitative mechanism that has been put forward to explain the up to 90% energy efficiencies that were demonstrated in the 70s and 80s.<sup>2–7</sup>

Having established that it is energetically attractive, we note that the plasma chemical approach for reduction of CO<sub>2</sub> is also inherently appropriate in the context of alleviating intermittency of sustainable energy sources. The main reason for this is the low “inertia” of a plasma reactor, *i.e.* the plasma can be turned off and on and the input power can be regulated quickly (sub-second time scale, no heating of *e.g.* catalytic surfaces is required) and thus can follow the availability of energy surpluses. Secondly, the reactor is compact and power (*e.g.* microwave) supplies are cheap (0.1 euro per W), thus the investment costs can be low enough to economically allow intermittent use. Both aspects are not self-evident for, *e.g.*, electrolysis installations.

Although the plasma chemical approach for CO<sub>2</sub> reduction has been proven to be promising in terms of energy efficiency, it is presently not clear how this holds under industrially relevant throughputs. Two aspects play a role here. Firstly, the highest (90%) energy efficiencies were achieved at only a moderate (20%) conversion efficiency. Conversely, the highest (90%) conversion efficiencies were

achieved at a moderate (20%) energy efficiency.<sup>1</sup> Secondly, these experiments were performed at a strongly sub-atmospheric pressure. At elevated pressures, the efficiency remained very low level, typically <10%.

A microwave plasma approach for CO<sub>2</sub> dissociation has been recognized as the most favourable in terms of energy efficiency.<sup>6,8</sup> It is generally assumed that this is due to a low reduced electric field and hence preferential vibrational excitation. In recent years, a number of attempts have been undertaken with microwave discharges to reproduce these record values, experimentally as well as numerically.<sup>8–12</sup>

This paper also focuses on a microwave approach for CO<sub>2</sub> dissociation. Simple molecular physics considerations are discussed to illustrate the different CO<sub>2</sub> dissociation pathways. Conversion and energy efficiency are determined (from Fourier transform infrared spectroscopy, FT-IR, measurements) in scans of power, gas flow and reactor pressure. The level of non-equilibrium is assessed on the basis of gas temperatures that are determined from Rayleigh scattering density measurements combined with reactor pressure readings. These experimental results are interpreted in a comparison with estimated reaction rates on the basis of electron energy distribution calculations with a Boltzmann solver. Finally, a novel methodology to enhance the non-equilibrium is proposed.

## 2 Vibrational *versus* electronic excitation – elementary molecular physics

We discern three reaction pathways that may be relevant under common low temperature plasma conditions as expected in microwave CO<sub>2</sub> plasma. Each has its own intrinsic energy efficiency. These pathways are schematically drawn in Fig. 1 and the (in-)efficiency of each pathway is indicated by the amount of energy that is intrinsically converted to heat.

Firstly, dissociation may occur due to step-by-step vibrational excitation (see Fig. 1a). The reaction products may be formed without a significant amount of kinetic energy and thus it is the desirable channel for CO<sub>2</sub> dissociation. As

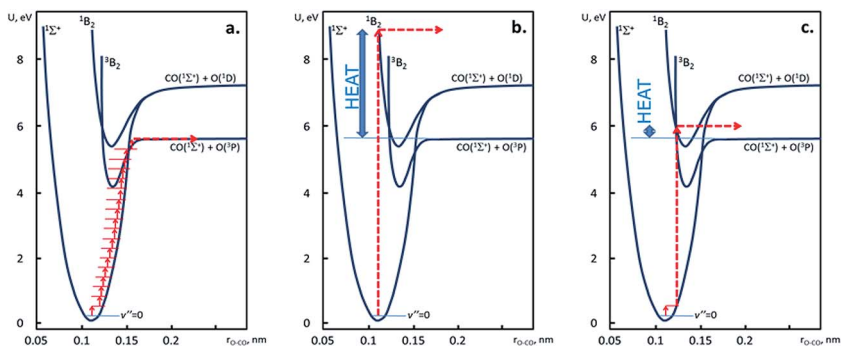


Fig. 1 Potential energy diagrams (as a function of one O–CO bond length) that illustrate the molecular physics behind three variants of CO<sub>2</sub> dissociation. Diagram (a) represents stepwise vibrational excitation that, after term crossing, causes ideally efficient dissociation. Contrary is the dissociative excitation in diagram (b), which involves a significant amount of heat to be released. A mix of these two cases is shown in diagram (c), vibrationally activated dissociative excitation, which is shown here as highly efficient as well.

mentioned before, this mechanism was put forward to explain the high energy efficiencies achieved. Typical electron temperatures of  $\sim 1$  eV ensure that a major portion of the discharge energy is transferred from the plasma electrons to the lower  $\text{CO}_2$  vibrational levels. At the same time, conversion of vibrational energy into translational energy can be kept to a minimum by ensuring a low gas temperature. Instead, vibrational–vibrational exchange may lead to overpopulation of the higher vibrational levels. The non-adiabatic transition  $^1\Sigma^+ \rightarrow ^3\text{B}_2$  opens the most effective dissociation pathway  $\text{CO}_2(^1\Sigma^+) \rightarrow \text{CO}(^1\Sigma^+) + \text{O}(^3\text{P})$ .

Secondly, dissociation may be induced by dissociative excitation (Fig. 1b). It is evident that this pathway involves the highest dissociation barrier and will be the least efficient. Electronic excitation becomes increasingly effective if the plasma temperature rises above  $\sim 1$  eV. This occurs for example when the input power exceeds the power loss to vibrational excitation (which leads to more electronic excitation upon an increase of the electron temperature).

Finally, vibrational stimulated electronic excitation (Fig. 1c) may occur as a mixture of the previous two. In the example sketched, a single vibrational excitation in the electronic ground state is sufficient to significantly decrease the excitation energy to the  $^1\text{B}_2$  upper state. Again, the non-adiabatic term crossing presents a dissociation pathway with 90% energy efficiency.

The plasma temperature (or more precisely, the electron energy distribution function) will in the end determine the relative importance of these reaction pathways as it determines the balance between vibrational excitations and electronic excitations.

## 3 Experimental

### 3.1 Microwave flow reactor

A 1 kW (continuous wave) microwave source is used to produce 2.45 GHz microwaves that are transferred through WR340 waveguides to the flow reactor (Fig. 2). A 3-stub tuner is placed in the microwave circuit to match the load impedance and adjust the power transfer. A sliding short is positioned a quarter wavelength away from the center of the quartz tube. A quartz tube, which is placed perpendicularly through the broad wall of the waveguide, serves as flow reactor. A 27 mm inner diameter tube was used during the Rayleigh scattering measurements while during the FTIR measurements a 18 mm diameter tube was used.

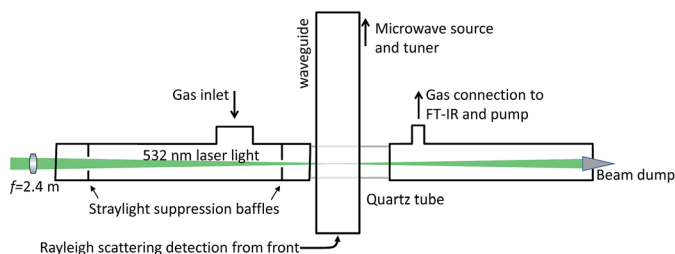


Fig. 2 Schematic of the microwave plasma source used for  $\text{CO}_2$  dissociation. Indicated is the laser beam path that is used for the Rayleigh scattering experiment.

Gas flows of up to 15 slm of pure CO<sub>2</sub> were supplied. The operation pressure in the reactor was independently controlled in the range of 10–250 mbar by varying the effective pumping speed.

### 3.2 Rayleigh scattering

A Nd:YAG laser light was used for the Rayleigh scattering measurements. The laser delivered 0.5 J per pulse at 532 nm with a repetition frequency of 10 Hz. An anti-reflection coated UV fused silica window was used to couple the laser into the reactor. A 2.4 m lens was used to focus the laser beam at the detection volume in the center of the waveguide. Since the divergence of the laser beam was 0.45 mrad, this resulted in a 1.1 mm diameter beam at the focus. A 20 mm diameter hole in the 14 mm thick sliding short enabled the observation of laser scattering with minimal microwave leakage.

To suppress parasitic scattering of the laser light, *e.g.* from imperfections in the entrance window, baffles were installed in the vacuum components. A critical aperture of 6 mm diameter was installed 505 mm from the scattering volume, and a subcritical aperture with 12 mm diameter was placed at 100 mm distance. The beam dump was placed 2 meters after the scattering volume, and was installed in a vacuum.

The magnification of the collection optics resulted in an axial detection range of approximately 20 mm. A fiber packet was used to transport the scattered light from the collection optics to the spectrometer, a single-pass spectrometer in Littrow arrangement with a 0.3 m focal distance Littrow lens. The spectrometer was equipped with a third generation image intensifier of type EPM102G-04-22S and a Manta-G145B camera.

### 3.3 FT-IR effluent measurements

FT-IR spectra were taken with a Varian 670 FTIR spectrometer at a resolution of 0.09 cm<sup>-1</sup>, so that individual ro-vibrational CO-peaks were resolved. A least square fit of the spectrum was used to obtain a species concentration *c* for different parameter settings using Beer–Lambert's law:

$$\ln\left(\frac{I}{I_0}\right) = -\varepsilon(p, T)cl. \quad (1)$$

The values for the molecule specific absorptivity  $\varepsilon$  were obtained from the HITEMP database,<sup>13</sup> where pressure and Doppler-broadening, as well as instrument-broadening are taken into account. The temperature was assumed to be constant at room temperature. Detailed fits showed this to be accurate within 15 K. At higher pressures and CO-concentrations, the most intense CO-peaks were saturated and thus disregarded in the fitting. The CO fraction *f* in the effluent was determined from the concentration and pressure, and subsequently converted into the conversion factor  $\alpha$  using the relation:

$$f = \frac{\alpha}{(1 + \alpha/2)}. \quad (2)$$

For conversions lower than 2%, the fitting routine didn't converge and a 'best-fit' was estimated by inspection. Knowing the conversion efficiency, the energy efficiency can be calculated using:

$$\eta = \frac{q\alpha E_{d,\text{CO}_2}}{P_{\text{in}}}, \quad (3)$$

where  $q$  is the gas flow rate in molecules per second,  $E_{d,\text{CO}_2}$  is the effective dissociation energy per  $\text{CO}_2$  molecule (2.9 eV) and  $P_{\text{in}}$  is the input power.

## 4 Experimental results

### 4.1 Discharge modes – spontaneous light emission

Depending on the operational conditions, particularly on the ratio between pressure and electric field, different modes of plasma operation are known to occur in microwave plasma discharges: diffuse, contracted, and a combination thereof.<sup>1</sup> The contracted plasma region forms at high electron densities. The high density prevents electromagnetic waves penetrating into the core of the plasma and, instead, the microwave power is absorbed in a skin layer at the boundary of the high density region. Generally, the plasma becomes also thermal in this mode, *i.e.* the neutral gas temperature approaches the plasma temperature. It is believed that a combined operation, in which the small volume of thermal plasma is surrounded by a large volume of non-equilibrium plasma, is best to achieve high energy efficiency conversion.

These different modes of operation and transitions in between occurred in the experiments that are discussed in this work as well. To illustrate the effect, images of the spontaneous light emission of the plasma inside the waveguide are shown in Fig. 3. The two cases differed mainly in reactor pressure and correspond to the extremes of the parameter space that was covered: 10 and 250 mbar (input power was 650 and 550 W, respectively; gas flow rate was 13 slm in both cases).

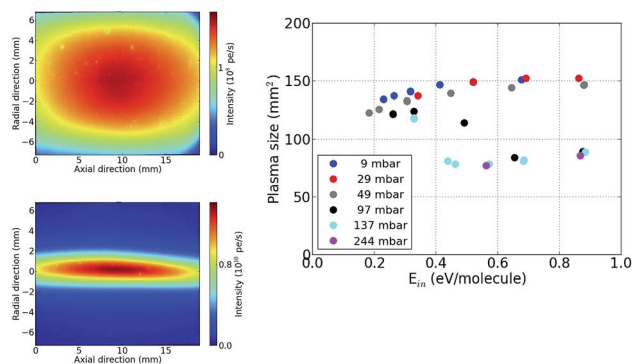


Fig. 3 Spontaneous light emission from the plasma inside the waveguide for (left top) 10 mbar (650 W, 13 slm) and (left bottom) 250 mbar (550 W, 13 slm), illustrating the two modes of operation: diffuse and contracted.<sup>1</sup> It is noted that vignetting at the sides of the images was not corrected for. The plot on the right shows the plasma cross sectional area determined from such emission images in dependence of pressure and specific energy. Plasma cross sectional areas of 120–150 mm<sup>2</sup> and 80 mm<sup>2</sup> correspond to diffuse and contracted operations, respectively.

The emission images were used to estimate the (cross sectional) plasma size in order to qualify the mode of operation throughout the parameter space covered by the present experiments. The results are presented in dependence of the specific energy input in the plot in Fig. 3. In essence, full width half maxima values were used. The plot clearly resolves the diffuse mode with typical plasma cross sectional areas of 120–150 mm<sup>2</sup> and the contracted mode with a size of typically 80 mm<sup>2</sup>. Reducing the specific energy input evidently causes back transition of the high pressure contracted mode to a high pressure diffuse mode.

## 4.2 Conversion degree and energy efficiency

The performance of microwave plasma dissociation of CO<sub>2</sub> was characterized firstly with respect to conversion degree ( $\alpha$ ). The conversion degrees were inferred from FT-IR measurements of the effluent. The results are plotted in Fig. 4 for scans of specific energy (input power, range 300–1000 W, divided by gas flow rate) and pressure (25–200 mbar) at gas flow rates of 5 and 15 slm. The following observations are made. (i) The pressure series that yield the highest conversions line up along a common linear dependence on the specific energy input. (ii) An optimum exists in operation pressure. This is most clearly seen for the 5 slm data, in which the 100 and 150 mbar series are at maximum conversion whereas the 37 and 200 mbar series show decreased performance. The 15 slm data step up in conversion as pressure goes up and reach a maximum for pressures of 150 and 200 mbar. The latter also implies that (iii) the optimum operation pressure shifts up with gas flow rate. Furthermore, returning to the previous discussion on the different modes of operation, (iv) it was observed that the highest conversion series all correspond to the plasma operating in the contracted mode. Finally, (iv) the high flow data peak at 0.8 eV per molecule energy input. We presently believe that this relates to a transition to the combined diffuse-contracted mode.

The same data is plotted in Fig. 5 in terms of energy efficiency for CO formation, this time with a logarithmic specific energy input axis. As to be expected, the trends are similar as before. Efficiencies range from 7% up to ~45%. In other words, the record high energy efficiencies of 90% are not reproduced in

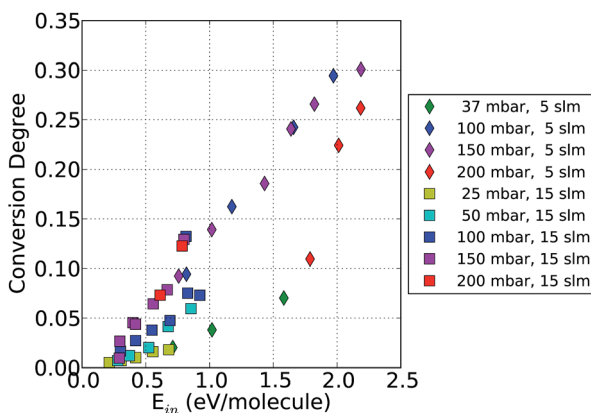


Fig. 4 Conversion degree measured in pure microwave CO<sub>2</sub> plasma as a function of the specific energy input, at 5 and 15 slm gas flow rate, in scans of the reactor pressure.

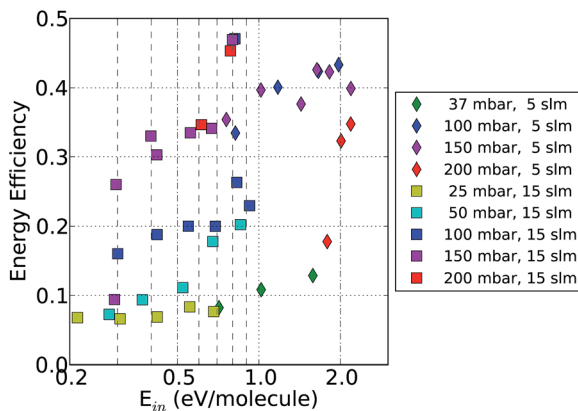


Fig. 5 Energy efficiency measured in pure microwave  $\text{CO}_2$  plasma as a function of the specific energy input, at 5 and 15 slm gas flow rates, in scans of the reactor pressure. The underlying experimental data are identical to those of Fig. 4.

the present experiments, although similar conditions in terms of pressure and specific energy were covered.<sup>2</sup>

### 4.3 Gas temperature

A signature of reaching the desired non-equilibrium conditions is a low gas temperature that is maintained whilst vibrational temperatures (up to 8000 K<sup>12,14</sup>) and plasma temperatures (1–5 eV) are high. Usually, rotational distribution temperatures are determined by molecular spectroscopy as a measure for the gas temperature. This assumes equilibration between rotational and translational degrees of freedom, which is not always necessarily the case.<sup>15</sup> In this work, we rely on direct, *in situ* and spatially resolved, density measurements with laser Rayleigh scattering, from which temperatures are inferred using reactor pressure readings and the ideal gas law. Taking the parameter space covered by the conversion measurements as reference, we selected a high and low pressure condition (20 and 135 mbar) at a high flow rate (13 slm) to perform scans of the specific energy. The temperature results are presented in Fig. 6.

In the analysis, pure  $\text{CO}_2$  was assumed as the scattering species. However, in the case of significant dissociation, considerable amounts of CO and  $\text{O}_2$  would also have been present. This would disturb the temperature analysis as the total Rayleigh scattering caused by CO and  $\frac{1}{2}\text{O}_2$  is a factor 1.5 less than the scattering from  $\text{CO}_2$ . So if locally all  $\text{CO}_2$  was dissociated, the temperature would be overestimated by the same factor of 1.5. A perhaps more realistic estimate of the maximum error is to assume at the highest specific energy input an energy efficiency of 50%, *i.e.* a maximum conversion degree of 15%. This would imply an overestimation of the neutral gas temperature of only 5%.

It is seen that gas temperatures are around 2000 K for the low pressure conditions but rise steeply to values that are usually assumed for the temperature of the plasma electrons for the high pressure conditions. Putting these observations in the context of the earlier conversion measurements: the highest conversions are obtained as gas temperatures are also maximal.



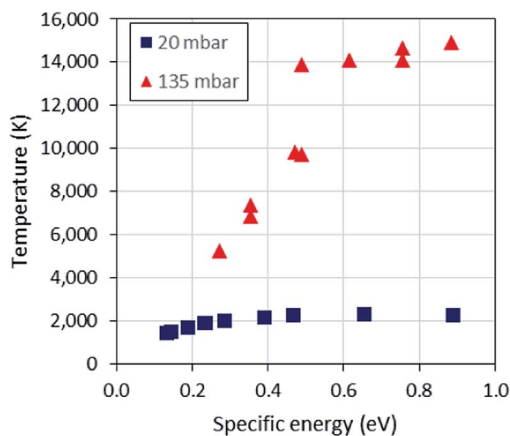


Fig. 6 Gas temperatures determined from neutral gas density measurements with Rayleigh scattering and reactor pressure readings in a scan of specific energy input. The gas flow was at 13 slm similar to the high flow conditions in Fig. 4 and 5, the pressure was tuned to 20 and 135 mbar, respectively.

The temperature data exhibit a sudden rise at a specific energy of about 0.5 eV. A closer inspection of the 137 mbar data series in the plot of the discharge cross sectional areas (Fig. 3) shows that this is exactly where the discharge undergoes a transition from diffuse to contracted. Apparently, contracted discharges have a central neutral gas temperature that is approximately constant at  $1.4 \times 10^4$  K.

## 5 Electron energy distribution evaluation

The temperature of the electrons, or equivalently the mean energy, in a discharge is set by the requirement that on average an electron should be able to replace itself by an ionization event before it escapes to the wall or it recombines with a positively charged heavy particle in the volume. In other words: the production by ionization must be equal to the losses, or, the electron temperature is determined by the particle balance. For a discharge as studied here (simplified in the following by a uniform electron density  $n_e$ , electron temperature  $T_e$ , and gas density  $n_0$  in a reactor of radius  $r$ ), we write the particle balance as:

$$n_e n_0 k_{\text{ion}}(T_e) = n_e^2 k_{\text{DR}}(T_e) + \frac{n_e c_s(T_e)}{2r}. \quad (4)$$

The left hand side (LHS) of the equation is the production of ions (with  $k_{\text{ion}}(T_e)$  the effective ionization rate per unit of volume). The first term on the RHS (right hand side) is volume recombination due to dissociative recombination, with the dissociative recombination rate  $k_{\text{DR}} = 4.2 \times 10^{-13} (T_e/300 \text{ K})^{-0.75} \text{ m}^3 \text{ s}^{-1}$ .<sup>16</sup> The second term indicates wall recombination due to Bohm flux to the wall, *i.e.* ions reach sound speed  $c_s$  at the sheath in front of the wall. Note that plasma flow is disregarded as typical flow velocities of 100–500  $\text{m s}^{-1}$  are negligible compared to the sound speed.

The electron density is determined by the requirement that the number of collisions between electrons and heavy particles is sufficient to transfer the power injected into the discharge,  $P_{\text{in}}$ , to the heavy particles. In other words, the electron density is determined by the power balance, which is written as:

$$\frac{P_{\text{in}}}{V} = n_e n_0 \sum_i (k_i U_i) \quad (5)$$

(with  $V$  the reactor volume and  $k_i$  and  $U_i$  the rate and energy loss of an energy transfer process). In the ideal case, vibrational excitation would dominate and would be the only term on the RHS.

In case of Maxwellian velocity distributions, these equations are straightforward to solve. However, the free electrons in microwave discharges are recognized to be more likely Druyvesteyn distributed.<sup>1</sup> This means that the high energy tail is decreased, which drives the mean electron energy up to still supply sufficient ionization. In such cases, a Boltzmann solver can be used to model the electron energy distribution function (EEDF), in which case effective rates of the relevant processes are calculated on a basis of the cross sections. The publicly available Bolsig<sup>+</sup> solver,<sup>17</sup> was used, which has been described by Hagelaar and Pitchford.<sup>18</sup>

The results of solving the balanced equations assuming Maxwellian distributions and EEDF calculations with Bolsig<sup>+</sup> are compared in Fig. 7. In the case of a Maxwellian distribution, the mean electron energy is taken as  $\frac{3}{2} k_B T_e$ . It is seen that the mean electron energy is indeed increased due to the non-Maxwellian nature of the discharge. Moreover, with increasing input power, the mean electron energy increases, thus opening direct electron excitation channels in addition to the preferred vibrational excitation.

At this point it is of interest to note that the mean electron energies calculated here are different from values that are calculated or estimated in other work,

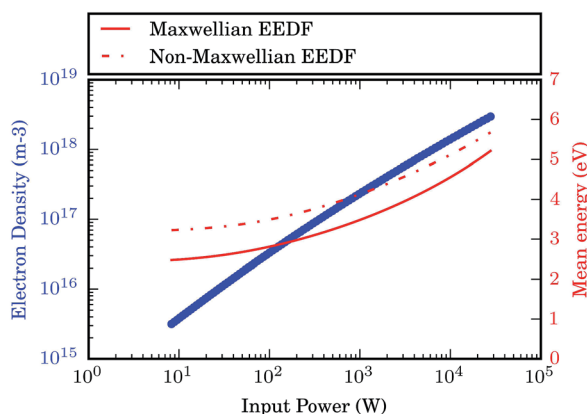


Fig. 7 Electron density (left axis) and mean energy (right axis) calculated as a function of input power for a CO<sub>2</sub> microwave discharge. Compared are solutions of the balanced equations assuming a Maxwellian EEDF and solutions which involved detailed Bolsig<sup>+</sup> calculations of the EEDF. The non-Maxwellian nature leads to increased mean electron energies. Dissociative recombination becomes more important as density increases, which causes the increase in mean electron energy with input power. Assumed was a neutral gas density of  $10^{23} \text{ m}^{-3}$ , which is similar to measured values.

*e.g.* by Kozák *et al.*<sup>8</sup> or Silva *et al.*<sup>12</sup> Usually, microwave discharges in CO<sub>2</sub> are assumed to operate at electron temperatures of 1–2 eV, *i.e.* mean energies of 1.5–3.5 eV. At modest power inputs of 10 W there is quantitative agreement with these literature values, but with increasing power, the mean electron energy increases significantly. One may be suspicious about the simplified wall losses in the particle balance that are used here (eqn (4)). After all, the electron density will in reality be lower near the walls compared to the center, especially in the contracted mode of operation, thus Bohm fluxes calculated on the basis that central densities overestimate the losses significantly. In fact, a radial ambipolar diffusion model (as used by *e.g.* Vijvers *et al.* for thermal arcs<sup>19</sup>) would have been more appropriate. This was not implemented since it is not significant compared to dissociative recombination. The main characteristic of dissociative recombination is its dependence on the square of the electron density (eqn 4). As a result, it causes the mean electron energy to increase with electron density, which is seen in Fig. 7. Already around an input power of 100 W, the electron energy is seen to increase, indicating that dissociative recombination is at play in the particle balance.

Knowing the EEDF enables calculation of the effective rates on the basis of the cross sections. These rates can be normalized to yield electron energy loss fractions giving more insight into the loss processes of the electrons. In Fig. 8 these loss fractions are shown for various processes. A major insight is obtained from this plot: the Bolsig<sup>+</sup> evaluations predict that at reactor relevant values of input power, the vibrational excitation is no longer dominant in the power balance. This is indirect, *via* increasing of the mean energy due to dissociative recombination.

Important in the present context is that dissociative recombination not only shortens the ion lifetime and therewith increases the electron energy, but also converts ionization energy into additional heating of the neutral gas. Since the vibration–translation exchange increases with gas temperature,<sup>20</sup> the extra gas heating might be sufficient to quench the vibrational excitation.

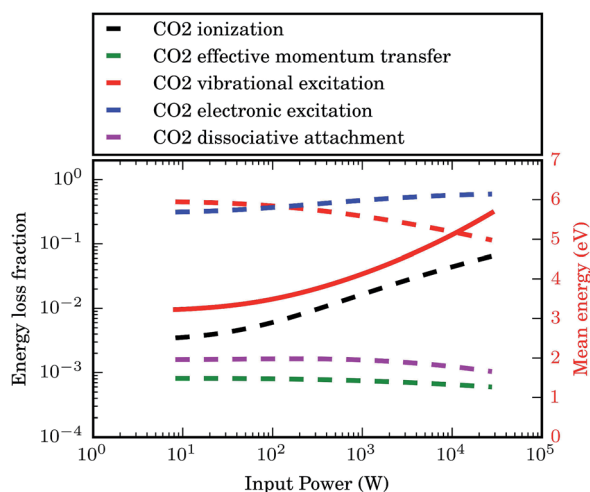


Fig. 8 Energy loss fractions for the various processes at play in a CO<sub>2</sub> microwave discharge. It shows that vibrational excitation is not the dominant energy loss channel for the electrons in conditions as investigated in the present work.

## 6 Discussion

Having explored  $\text{CO}_2$  dissociation in microwave plasma both experimentally in terms of dissociation degree, energy efficiency, and neutral gas temperature, as well as numerically in terms of EEDF and energy loss fractions for the main reaction processes at play in the plasma, we summarize the main findings as follows:

- the energy efficiency for CO formation never exceeded the thermodynamic equilibrium value of  $\sim 45\%$  in the investigated pressure range;
- the conversion degree for CO formation never approached the thermodynamic maximum of  $\sim 55\%$ ;
- the best performance was observed at pressures of around 150 mbar and also when the plasma operated in the contracted mode (in which gas temperatures in the center are too high to expect strong non-equilibrium conditions in view of vibration-to-translation relaxation);
- the electron energy estimates indicate that vibrational excitation is not dominant in the present conditions.

In other words, it is questionable whether vibrational excitation has been at play in the present experiments. Here, we will put these findings in the context of thermal equilibrium dissociation efficiencies, hypothesize on the mechanism of dissociation at play and how this relates to the observed scalings of dissociation degree and energy efficiency with input power.

As reference, thermodynamic equilibrium conversion data were calculated with the CEA package,<sup>21</sup> which are plotted in Fig. 9. Also included in the plot are energy efficiencies calculated assuming instantaneous cooling.<sup>22</sup>

Let's first put the *in situ* temperature measurements (Fig. 6) in the context of the chemical equilibrium data. Starting with the low pressure series (20 mbar, in a diffuse discharge mode), which were rather constant at around 2000 K, these

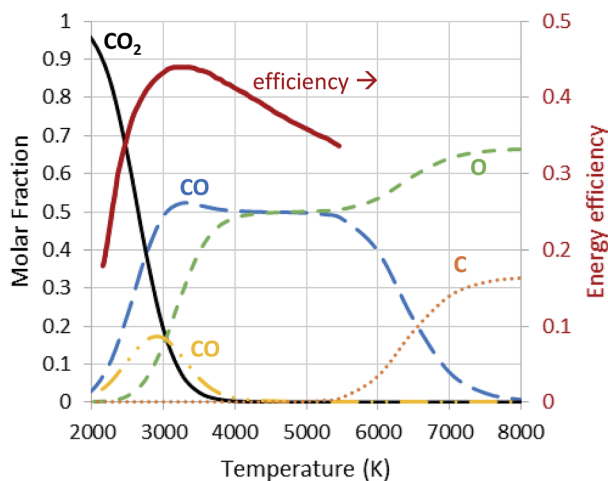


Fig. 9 Chemical equilibrium calculated molar fraction of the products of  $\text{CO}_2$  dissociation at a fixed pressure of 100 mbar. Calculated energy efficiencies assuming instantaneous quenching after Polak *et al.* are plotted on the right axis.

would produce chemical equilibrium conversion degrees of about 5%. The measured data at a similar pressure (25 mbar, Fig. 4) increased with power from close to zero to up to ~2%. These measured conversion degrees thus make perfect sense if one realizes that the radial temperature must have peaked. As a result of the peaking, only the hotter centers would have contributed to dissociation. At increasing input power the radius of the dissociation zone would have increased thus producing more dissociation and hence the measured linear behavior.

Next is the high pressure series (135 mbar). The measured temperatures in the center of these contracted discharges started at 5000 K and increased to over 15 000 K. In terms of chemical equilibrium conversion, this corresponds to starting at a maximum conversion of 50% that subsequently drops down to 0% CO due to full dissociation. The measured conversions, however, go up from a few % to nearly 10%. The same temperature peaking argument holds again. However, this time the CO formation region moves out of the center as the temperature increases beyond the CO formation region. This extra hot center becomes even smaller as the discharge contracts. In this situation, the plasma acts as a central heat source that provides the outer regions with thermal heat and induces the dissociation. The amount of gas in the extra hot center is relatively small. Not only does geometry play a role here (the central cross section being smaller than the boundary area), but also the strong temperature peaking in the center in radially constant pressure implies rarefaction of the center.

An aspect that has not been considered in the present work is the quenching of the reaction products. In fact, no measures had been in place to optimize the quenching rate. Instead, the effluent had been flowing through a constant radius tube, only being cooled by the colder tube walls. Roughly estimating, this gives a quenching rate of only  $10^6 \text{ K s}^{-1}$  (assuming 1000 K cooling over 10 cm with a flow velocity of  $100 \text{ m s}^{-1}$ ). As a consequence, back reactions might have deteriorated energy efficiencies in the effluent by a factor of more than 2 compared to inside the reactor.

These equilibrium features of the observed dissociation degrees are in line with the mean electron energy evaluations and the consequence that vibrational excitation is not the main electron energy loss process. However, both aspects are especially valid for the central regions of the reactor, *i.e.* the hotter plasma region and its direct hot neutral gas surroundings. So the non-equilibrium dynamics may still be at play further out, even closer to the reactor walls where the gas is colder and still an appreciable density of low energy electrons is available for vibrational excitation. Indeed, closer inspection of the energy efficiencies that are presented in Fig. 5 do show a sign thereof. Especially the outliers at about 0.8 eV specific energy, which were already indicated to correspond to the combined diffuse-contracted mode, point to partly non-equilibrium CO production. The achieved energy efficiency of just over 45% approaches the maximum of the calculated efficiency for instantaneous quenching (see Fig. 9), and it is thus improbable that this could have been achieved by thermal equilibrium chemistry alone in the present reactor geometry.

Having established that thermodynamic equilibrium chemistry dominates in the present work, the question arises how to move in operational space to strong non-equilibrium dominated conditions. One aspect that should help in this respect is lowering the pressure even further, to the 1 mbar range, *e.g.* by installing larger diameter flow tubes. This is based on the one hand on

observing lower neutral gas temperatures at lower pressure, and on the other hand on dissociative recombination strongly falling off with electron density. In the next Section, we propose an alternative, entirely novel, approach that relies on tailoring the EEDF by adding low ionization potential species to the reactor input.

## 7 Adding traces of low ionization potential alkali metals

Having established that the mean electron energy has been too high for preferential vibrational excitation leading to a strong non-equilibrium, the relevant question to ask is how to mitigate this effect induced by dissociative recombination. In other words, how to tame the  $\text{CO}_2$  microwave discharge? We postulate that this can possibly be achieved by adding traces of low ionization potential species, *e.g.* alkali metals such as lithium, sodium or potassium. The effect of this action will be twofold. Firstly, the lower ionization potential will cause a lower plasma temperature *via* the particle balance. Secondly, the positive charge is no longer carried by molecular ions, so that volume recombination *via* dissociative recombination is no longer at play. Atomic ions can only recombine in the volume *via* three-body recombination, a process which has exceedingly small reaction rates. In the absence of dissociative recombination, the previously observed electron density dependence on the mean electron energy, as shown in Fig. 7, will vanish.

To estimate the effect of seeding sodium to the discharge, the addition of alkali impurities was modeled using Bolsig<sup>+</sup>. Firstly, the calculated electron density and mean energy are presented as a function of input power in Fig. 10. It is seen that the mean electron energy is indeed significantly decreased, to 1 eV (*i.e.* in the case of a near Maxwellian distribution, this would mean 0.7 eV electron temperature) and its previous dependence on electron density (or input power) is no longer present.

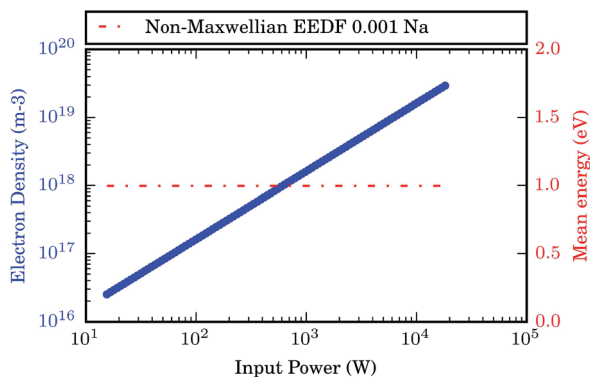


Fig. 10 The effect of sodium being added to a  $\text{CO}_2$  microwave discharge on the mean electron energy as calculated with the Bolsig<sup>+</sup> solver. Assumed was 0.01% sodium added to a neutral gas density of  $10^{23} \text{ m}^{-3}$ . The mean electron energy is significantly decreased and lost any dependence on input power (compared to Fig. 7).

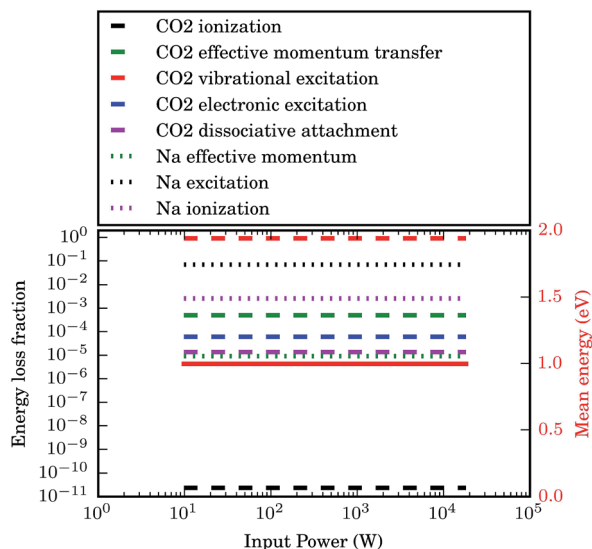


Fig. 11 The effect of 0.01% sodium added to a CO<sub>2</sub> microwave discharge on the relative energy loss fractions for the main processes at play. It shows that vibrational excitation has become the dominant energy loss channel for the electrons, which does not change within the conditions investigated in the present work.

As the mean electron energy has become independent of input power, so have the energy loss fractions, as can be seen in Fig. 11. More importantly, vibrational excitation has become the dominant energy loss channel for the electrons. In other words, these evaluations support the beneficial effect of adding low ionization species for reaching a strong non-equilibrium in a CO<sub>2</sub> microwave discharge.

An important result from analyzing the energy loss fractions is that adding sodium at amounts of 0.01% (which allows equal levels of ionization degree) does not add a significant amount of radiative losses to the power balance. This becomes important at levels of 0.1–1% and thus sets the limit on the amount of sodium that can be added. It is noted that this balance may be different for other alkali metals.

## 8 Conclusions

The present experiments and EEDF evaluations show that retaining a low electron temperature (mean energy) is required for realizing strongly non-equilibrium conditions that yield high energy efficiency CO<sub>2</sub> conversion. One possible route to follow is enhancing the volume of the non-equilibrium regions in the reactor compared to the high density chemical equilibrium plasma part. However, this will always mean compromising between high power input (*i.e.* reaching application relevant throughput) and achieving high efficiency. A successful development of the here proposed alkali additives would offer an alternative in which the plasma dynamics can be tailored to the non-equilibrium in the entire discharge volume. In effect, it would overcome the compromise, the trade-off between

conversion degree and energy efficiency. It would tame the microwave plasma to beat thermodynamic equilibrium performance in CO<sub>2</sub> dissociation.

## References

- 1 A. A. Fridman, *Plasma Chemistry*, Cambridge University Press, New York, 2008.
- 2 R. I. Azizov, A. K. Vakar, V. K. Zhivotov, M. F. Krotov, O. A. Zinov'ev, B. V. Potapkin, V. D. Rusanov, A. A. Rusanov and A. A. Fridman, *Sov. Phys. Dokl.*, 1983, **28**, 567.
- 3 I. A. Semiokhin, Y. P. Andreev and G. M. Panchenkov, *Russ. J. Phys. Chem.*, 1964, **38**, 1126.
- 4 A. N. Maltsev, E. N. Eremin and L. V. Ivanter, *Russ. J. Phys. Chem.*, 1967, **41**, 633.
- 5 Y. P. Andreev, I. A. Semiokhin, Y. M. Voronkov, V. A. Sirotkina and V. A. Kaigorodov, *Russ. J. Phys. Chem.*, 1971, **45**, 1587.
- 6 V. D. Rusanov, A. A. Fridman and G. V. Sholin, *Sov. Phys.-Usp.*, 1981, **24**, 447.
- 7 R. I. Asisov, A. A. Fridman, V. K. Givotov, E. G. Krashenninikov, B. I. Petrushev, B. V. Potapkin, V. D. Rusanov, M. F. Krotov and I. V. Kurchatov, *5th Int. Symp. on Plasma Chemistry*, Scotland, Edinburgh, 1981, p. 774.
- 8 T. Kozák and A. Bogaerts, *Plasma Sources Sci. Technol.*, 2015, **24**, 015024.
- 9 L. F. Spencer and A. D. Gallimore, *Plasma Chem. Plasma Process.*, 2011, **31**, 79.
- 10 L. F. Spencer and A. D. Gallimore, *Plasma Sources Sci. Technol.*, 2013, **22**, 015019.
- 11 A. Goede, W. A. Bongers, M. F. Graswinckel, M. C. M. van de Sanden, M. Leins, J. Kopecki, A. Schulz and M. Walker, *3rd European Energy Conf.*, Hungary, Budapest, 2013.
- 12 T. Silva, N. Britun, T. Godfroid and R. Snyders, *Plasma Sources Sci. Technol.*, 2014, **23**, 025009.
- 13 L. S. Rothman, I. E. Gordon, R. J. Barber, H. Dothe, R. R. Gamache, A. Goldman, V. I. Perevalov, S. A. Tashkun and J. Tennyson, *J. Quant. Spectrosc. Radiat. Transfer*, 2010, **111**, 2139–2150.
- 14 A. K. Vakar, V. K. Zhivotov, F. F. Karimova, E. G. Krashenninikov, V. D. Rusanov and A. A. Fridman, *Sov. Tech. Phys. Lett.*, 1981, **7**, 429.
- 15 N. den Harder, D. C. Schram, W. J. Goedheer, H. J. de Blank, M. C. M. van de Sanden and G. J. van Rooij, *Plasma Sources Sci. Technol.*, 2015, **24**, 025020.
- 16 A. A. Viggiano, A. Ehlerding, F. Hellberg, R. D. Thomas, V. Zhaunerchyk, W. D. Geppert, H. Montaigne, M. Larsson, M. Kaminska and F. Österdahl, *J. Chem. Phys.*, 2005, **122**, 226101.
- 17 <http://www.bolsig.laplace.univ-tlse.fr/>.
- 18 G. J. M. Hagelaar and L. C. Pitchford, *Plasma Sources Sci. Technol.*, 2005, **14**, 722.
- 19 W. A. J. Vijvers, D. C. Schram, A. E. Shumack, N. J. L. Cardozo, J. Rapp and G. J. van Rooij, *Plasma Sources Sci. Technol.*, 2010, **19**, 15.
- 20 E. Treanor, J. W. Rich and R. G. Rehm, *J. Chem. Phys.*, 1968, **48**, 1798–1807.
- 21 S. Gordon and B. J. McBride, *Computer Program for Calculation of Complex Chemical Equilibrium Compositions and Applications II: Users Manual and Program Description*, NASA Reference Publication, 1996, vol. 1311.
- 22 A. A. Fridman, in *Plasma Chemistry*, Cambridge University Press, New York, 2008, p. 263, Fig. 5–4.